Mapping Altered Rocks Using Landsat TM and Lithogeochemical Data: Sulphurets-Brucejack Lake District, British Columbia, Canada

J.R. Harris, A.N. Rencz, B. Ballantyne, and C. Sheridon

Abstract

Landsat Thematic Mapper (TM) data have been used to detect the presence of altered rocks associated with ore mineral deposition. In arid environments, the spectral signatures of diagnostic minerals are often not masked by water, vegetation, or surficial materials. There are many studies in which TM data have been used to locate hydrothermally altered rocks in near desert regions, but few successful examples can be found that relate to glaciated, vegetated terrain at high latitudes. In this paper, TM data, in concert with lithogeochemical data and field observations, are used to detect and map altered rocks in the Sulphurets-Brucejack Lake district of northwestern British Columbia.

Areas of iron-pyrite and phyllic (sericitic) alteration as well as areas of intense silicification have been located using band ratioing techniques. The chemical nature of these alteration zones has been established through comparison with lithogeochemical data. These alteration styles reflect the underlying rock type, as would be expected, but also appear to reflect two different styles of alteration, perhaps reflecting different mineralizing systems. The western half of the study area, characterized by iron-pyritic alteration, reflects a base metal (Cu porphyry and minor Au) system while the eastern half, characterized by areas of silicification and clay alteration, may represent a precious metal (Au, As, Sb) system.

Introduction

Many researchers have used remotely sensed data to investigate the presence of alteration mineral assemblages within rocks that have undergone hydrothermal fluid affects associated with ore mineral deposition. Specific alteration mineral assemblages in turn can provide direct evidence of mineralization. Spectral variations associated with altered rocks caused by hydrothermal fluids can, in some cases, be detected on Landsat Thematic Mapper (TM) imagery (Goetz, 1989). The main application of remote sensing technology for mapping altered rocks has been the detection of various alteration styles in the visible through the short wavelength infrared portion of the electro-magnetic spectrum.

In the spectral range of 0.4 μm to 1.1 μm, spectral reflectance data from labratory analysis have been used to determine the presence of iron oxides and hydroxides such as limonite and goethite. Limonite and goethite in the surficial environment are significant because they are the oxidation products of various sulphide ore minerals. The disseminated nature of sulphide minerals within alteration haloes of most ore deposits may provide clues to blind mineralization. Therefore, the detection of leached products of sulphides, i.e., limonite and goethite (gossans), can be direct exploration guides.

In the 1.0- to 2.5-μm range, spectroscopy data have been used to identify hydrous minerals such as sericite, phyllosilicates, clay minerals, mica, and some sulfates. These minerals often constitute phyllic and argillic alteration and are particularly important as exploration guides for copper porphyry and precious metal deposits.

The aforementioned spectral ranges are covered by the TM sensor and have been successfully used in arid environments to map altered rocks (Abrams *et al.*, 1984; Goetz, 1989; Rowan and Lathram, 1980; Abrams *et al.*, 1977; Hunt and Ashley, 1979; Marsh and Mckeon, 1983; Elvidge and Lyon, 1984; Miller and Elvidge, 1985; Krohn, 1986).

Objectives

The primary objectives of the research reported here are

- to investigate the use of Landsat Thematic Mapper (TM) and ancillary lithogeochemical data for identifying and mapping altered rocks,
- to calibrate and verify the results obtained from the TM data using lithogeochemical data and field measurements, and
- to identify potentially mineralized areas for exploration follow-up using GIS modeling techniques.

Study Area

The study focuses on the Sulphurets-Brucejack Lake district in the Cordillera (mountains) of central-northwestern British Columbia where regional-scale expressions of Cu-Au porphyry systems are exposed at the present day surface (Ballantyne, 1990; Harris and Ballantyne, 1992; Kirkham and Margolis, 1995; Fowler and Wells, 1996; Margolis and Britten, 1996).

The Sulphurets district is located in the northwest corner of British Columbia on the east side of the Coast Mountains approximately 65 kilometres northwest of Stewart (Figure 1). The study area is mountainous, heavily glaciated, and largely covered by a mixture of coniferous vegetation and alpine grass as well as glacial ice. Exposed rock covers approximately 26 percent of the study area. Vegetation types and densities are largely controlled by elevation with dense coniferous vegetation covering the lower valleys and sporadic alpine flora at higher elevations. Exposed rock and soil are found on the flanks and tops of mountains.

The study area lies within the western portion of Stikinia, which is the largest of several tectonic terranes in the In-

Geological Survey of Canada, 615 Booth Street, Ottawa, Ontario K1A 0E9, Canada (harris@gis.nrcan.gc.ca).

Photogrammetric Engineering & Remote Sensing, Vol. 64, No. 4, April 1998, pp. 309–322.

0099-1112/98/6404–309$3.00/0

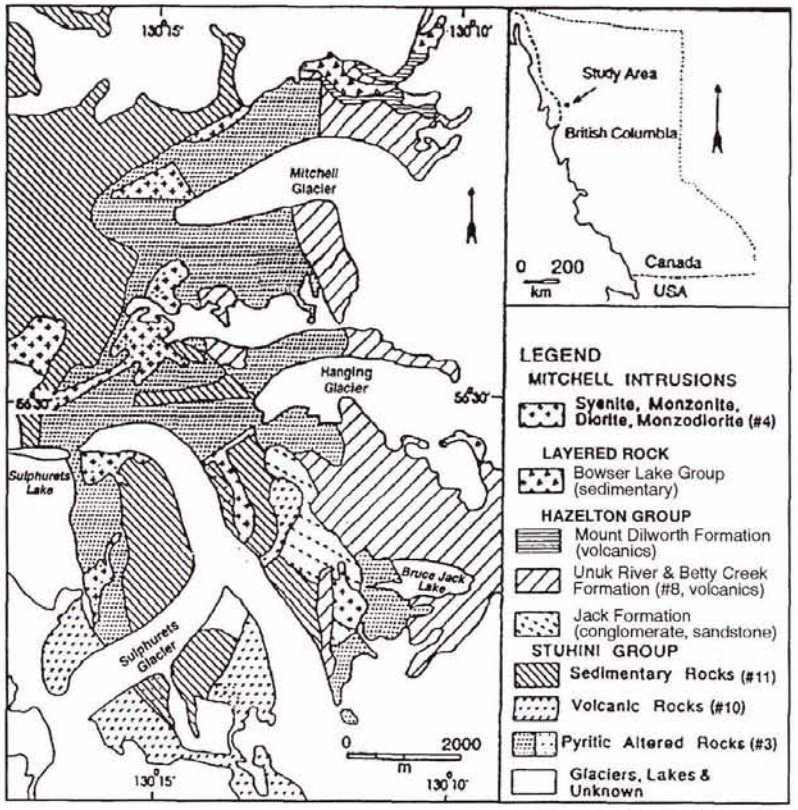

Figure 1. Simplified geological map of the Sulphurets district (from R.V. Kirkham, GSC)(#3 - #10) - geologic units.

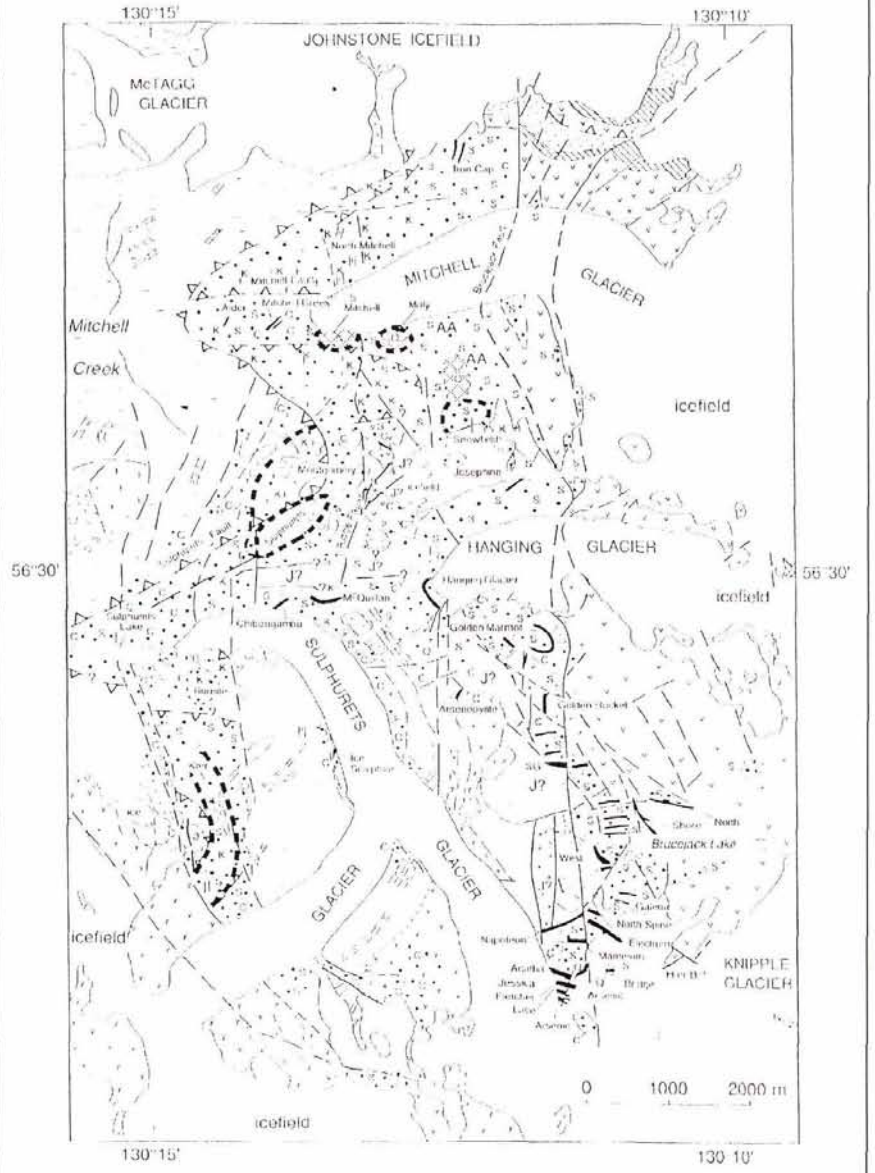

Figure 2. Detailed geology, alteration, and mineralization (ref derived from Figure 9A, p. 480, Kirkham and Margolis, 1995).

Figure 3. Landsat TM Band 5.

termontane Belt thought to have accreted to the North American continental margin in the middle Jurassic (Kirkham and Margolis, 1995). The area is underlain by Lower to Middle Jurassic volcanic and sedimentary rocks that have been affected by folding, faulting, and low grade regional metamorphism, primarily during the Cretaceous (Kirkham, 1963; Alldrick and Britton, 1988; Henderson *et al.*, 1992; Margolis, 1993). The generalized stratigraphic units are presented on Figure 1.

A Late Jurassic through Late Cretaceous tectonic event resulted in a generally east-verging fold and thrust belt which has affected much of the region (Evenchick, 1991). The Sulphurets and Mithchell thrust faults (Figure 2) postdate mineralization and locally juxtapose deeper parts of hydrothermal systems above shallower parts (Kirkham and Margolis, 1995). Many later northerly trending faults, including the Brucejack Fault, cut thrust faults and alteration zones. A late postmineral cleavage of variable orientation affects both altered and unaltered rocks (Kirham, 1963; Margolis, 1993; Bridge, 1993).

The strata are cut by at least three intrusive episodes which took place between Jurassic and Tertiary times (Alldrick and Britton, 1988). The western portion of the study area contains the majority of the intrusive rocks (Mithchell Intrusions) which include relatively large granitic intrusions and smaller dioritic intrusions in the southwest. Many of these intrusions show a close spatial and temporal relationship to porphyry copper and gold mineralization (Kirkham and Margolis, 1995).

Intense hydrothermal alteration is pervasive throughout the study area (Figure 2). Large zones of sericitic (phyllic) and pyritic alteration varying in width from a few metres to several hundred metres are present primarily in the eastern portion of the study area. Potassic feldspar (biotite, magnetite, hematite) alteration is pervasive in the western portion of the study area. The resultant altered rock is a foliated to schistose, quartz-pyrite-sericite rock with variable amounts of carbonate (Alldrick and Britton, 1988). The limonitic stains on the quartz-pyrite-sericite schists result from oxidization of the pyrite. Extensive zones of silicification manifested as quartz veining are also present in the eastern half of the study area.

In recent years, the Sulphurets-Brucejack Lake district has been the focus of important and intensive exploration for both precious metal (gold, silver) and porphyry copper deposits. Mineralization has been episodic, and various alteration and deposit styles are known to overlap as the result of structural complexities (juxtapositioning through faulting). The area is noted for extensive alteration zones associated with copper-gold and molybdenum porphyry systems as well as gold and silver mineralization (Alldrick and Britton, 1988). Porphyry copper-gold deposits and occurrences are found in the western half of the study area and include the Kerr, Sulphurets, Montgomery, Mitchell and North Mitchell (Figure 2). The Snowfield zone is a disseminated gold deposit in sericite-chlorite-pyrite altered basalt (Margolis and Britton, 1995). Gold-silver quartz veins that show evidence for brittle-ductile conditions of formation are found in the Brucejack Lake (West Zone) district in the eastern portion of the study area.

It is important to note that, with the severe local climate and steep relief typical for this part of British Columbia, there is only limited lichen growth on the rock outcrop, and surficial cover is largely absent. Large areas of exposed bedrock occur where reflectance is not masked by a vegetative and/or glacial cover. Consequently, this site provides the opportunity to investigate the application of TM for detecting hydrothermally altered exposures of bedrock. This continues some of the previous work conducted by Rencz *et al.* (1994a), Ballantyne and Ma (1992), and Ma *et al.* (1988) who have found TM data to be quite useful for mapping alteration zones in the area.

Data Processing

Data processing was accomplished using a variety of software tools including the PCI image analysis system (IAS), Arc/Info geographic information system (GIS), and the S-PLUS statistical analysis package. The IAS was used to process the TM data whereas the GIS was used to interpolate the various lithogeochemical datasets (e.g., produce continuous surface maps) and integrate and analyze the data. The statistics were calculated using a combination of the IAS and GIS as well as the statistical analysis package. Data transfer between the various software packages was trivial and involved the transfer of raster data as binary grids and point data as simple ASCII files.

Landsat

The study area is covered by Landsat TM scene 50555-191758, quadrant 4, which was recorded on 7 September 1985 and was obtained from Radarsat International (RSI). The image was chosen because it was essentially cloud free and at this time of year shows minimal seasonal snow cover; thus, the maximum amount of rock outcrop is exposed. Figure 3 shows a TM band 5 image of the study area. Generally, brighter tones indicate areas of rock outcrop.

Figure 4 is a summary of the processing steps applied to the TM data. Preprocessing steps involved georeferencing the data to a UTM topographic map base utilizing a series of ground control points and a second-order polynomial transform as well as correcting for atmospheric scattering using methods outlined by Crippen (1987). Correcting the shorter wavelength bands (e.g., TM bands 1, 2, and 3) for atmosphe-

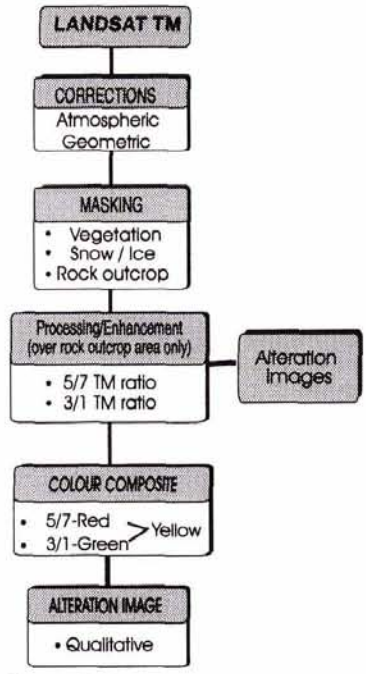

Figure 4. Landsat processing methodology.

ric scattering is critical, especially if band ratios are to be employed for locating altered rocks (see Crippen, 1988). Geometric rectification and adjustments for atmospheric scattering are standard corrections applied to TM data before analysis (Campbell, 1987; Drury, 1987; Sabins, 1996) and therefore will not be discussed further here.

Based on theoretical spectral curves, several techniques have been developed to identify alteration zones on TM imagery. These include principal component analysis, band ratio combinations, and various classification techniques (Abrams *et al.*, 1984; Buckingham and Sommer, 1983; Elvidge and Lyon, 1984). In this paper emphasis is placed on simple band ratios that have been effective for mapping altered rocks. Ratio images are created by dividing one TM channel (band) by another channel and then scaling the result for display purposes. Ratios are extremely useful for evaluating the spectral properties of earth materials by revealing reflectance differences between bands as well as minimizing brightness variations due to albedo and topographic slope (Rowan and Lathram, 1980). Ratioing is more "tractable" than other more complex image processing techniques such as principle component analysis because the resulting digital numbers (DN) can be readily related to the raw data.

Rock Outcrop Masking

Before proceeding with the calculation of ratio images, areas of outcrop and vegetation were delineated. This was accomplished by a series of simple image processing procedures through which all surface types including vegetation, glacial ice, glacial till, and rock outcrop were identified. A vegetation mask was created using a biomass ratio (TM band 4/3) to

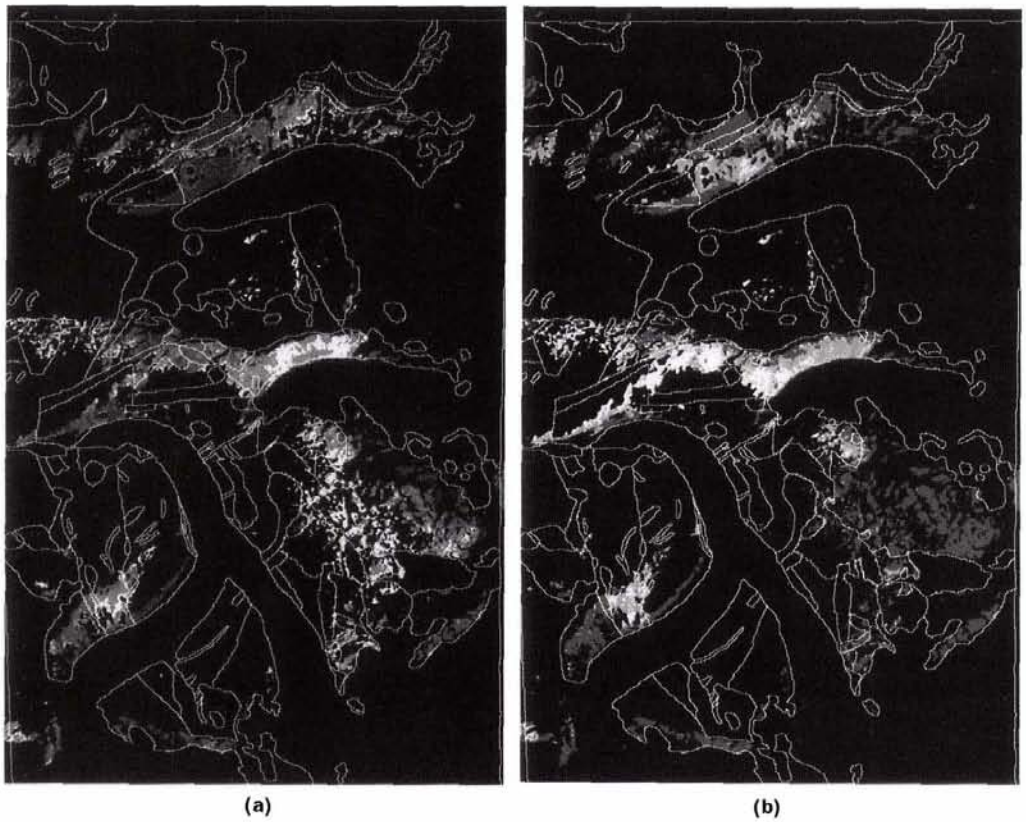

(a) (b)

Figure 5. (a) Landsat 5/7 ratio. (b) Landsat 3/1 ratio. Each ratio image has been divided into four classes based on standard deviation values as discussed in the text. The lighter tones represent higher ratio values reflecting more intense alteration. Lithological boundaries have been overlaid.

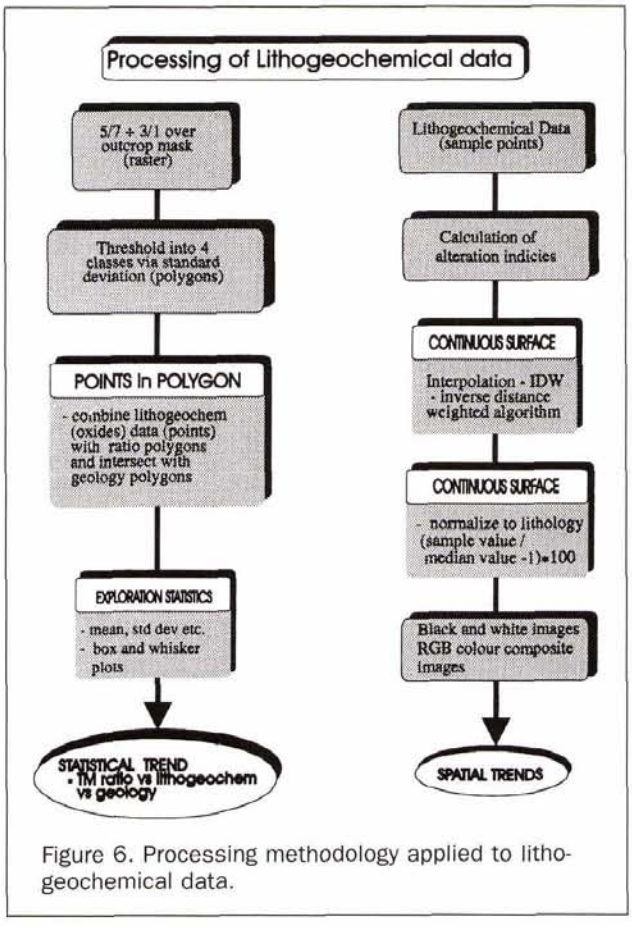

Figure 6. Processing methodology applied to lithogeochemical data.

differentiate between vegetated and non-vegetated areas. This ratio image was then interactively density sliced to produce the vegetation theme mask. The vegetation mask was then overlaid on a TM contrast stretched false color composite (bands 4, 3, and 2 displayed as red, green, and blue, respectively) to verify the accuracy and extent of the mask with respect to vegetated areas which show as red on this type of false color composite image.

Rock outcrop is quite reflective in the 1.6-μm range of the electromagnetic spectrum and, because TM band 5 coincides with this wavelength, the high reflectance areas from this band were extracted by thresholding (density slicing of the reflectance histogram) the upper portion of the data histogram. This mask was then intersected with the vegetation mask using a Boolean operator ("XOR") to eliminate areas that were confused with vegetation. All further image processing and statistical analysis was applied to the areas identified as rock outcrop through this masking procedure. The TM ratio images discussed below show areas of outcrop only.

Ratio Images

A TM 3/1 ratio image will highlight rocks that have been subjected to oxidation of iron bearing sulphides (typically pyrite and chalcopyrite, in this study area) because altered rocks are more reflective than unaltered rocks in TM Band 3 and less reflective in TM Band 1 due to iron absorption. The ratio image will accentuate the difference between the two bands with higher ratio values (brighter image tones), possibly representing areas of more intense iron sulphide oxidation. Similarly, a ratio of TM 5/TM 7 will highlight areas of possible sericite (phyllic) alteration as altered rocks are highly reflective in Band 5 and will have lower reflectance in Band 7 due to the presence of hydrous minerals. Figures 5a and 5b show the TM 5/7 and 3/1 ratio images over rock outcrop, respectively. The brighter tones potentially represent areas of more intense alteration whereas areas of darker tones represent areas of less intense alteration. Geological contacts have been overlaid on these images.

Based on these ratio images, a variety of color maps can be produced using IAS software to qualitatively display different alteration types in specific colors. Plate 1 is a two-component color image composed of the TM 5/7 ratio in red and the TM 3/1 ratio in green. The two channels have been normalized to the same mean and standard deviation. The resulting image indicates the presence of hydrous minerals in red whereas green indicates areas of leached and oxidized iron bearing minerals and yellow (e.g., red plus green) indicates the occurrence of hydrous minerals (e.g., sericite) plus iron oxidation of sulphides.

Lithogeochemical Data

Approximately 1000 lithogeochemical surface bedrock samples were collected between 1986 and 1990 by the Geological Survey of Canada (Kirkham *et al.*, 1990; Kirkham *et al.*, 1992) over accessible altered and unaltered rock. The samples (11 oxide elements and 34 trace elements) were analyzed by neutron activation (INAA), induced coupled plasma (ICP), and X-ray fluorescence (XRF) geochemical analysis techniques.

Figure 6 summarizes the processing steps applied to the lithogeochemical data. The TM ratio images (Figures 5a and 5b) were classified into four ratio classes based on standard deviation classes (≤ mean value, mean to mean + 1 standard deviations (sd), +1 to +2 sd, and > 2 sd). A "point in polygon" operation was performed within the GIS to intersect the ratio classes with the mapped geological units and lithogeochemical sample points. Only the oxide elements and selected trace elements were analyzed with respect to the underlying geology and ratio classes. First-order statistics and exploratory "box and whisker" plots were then calculated for each combination of the intersected categories to assist in the statistical comparison between the TM ratio classes and lithogeochemical data.

A number of alteration indices were calculated from the lithogeochemical data using the database software utilities within the GIS (Arc/Info) to assess the alteration patterns mapped from the TM ratio data. These indices included

- Sericite Index: $(K_2O/Na_2O + K_2O)$
- Chlorite Index: $(Fe_2O_3 + MgO/(Fe_2O_3 + MgO + CaO + Na_2O)$
- Alkali Index: $(Na_2O + CaO)/(Na_2O + K_2O + CaO)$
- Iron Index: Fe_2O_3/FeO

The sericite index emphasizes areas characterized by enriched potash (K_2O) reflecting sericitic alteration whereas the chlorite index emphasizes possible areas of more intense chloritization typified by higher ferrous iron and magnesium concentration. The alkali index emphasizes areas of alkali enrichment but can also serve to delineate areas of alkali depletion (lower index values) often associated with base metal and precious metal systems. The iron index which uses the ratio of ferrous to ferric iron can potentially emphasize areas of more intense iron oxidation (e.g., ferrous to ferric iron as result of oxidization).

A series of continuous surface maps of various oxide elements and alteration indices were calculated to establish spatial patterns present in the lithogeochemical data with respect to the TM ratio images. An inverse-distance weighted algorithm (Davis, 1986) was used to interpolate the data. The data were then normalized with respect to each lithological unit by calculating the median value of each oxide element for each lithology and then dividing each sample that intersected a given lithological unit by its median value. The normalizing formula (Gibson *et al.*, 1994) is shown below:

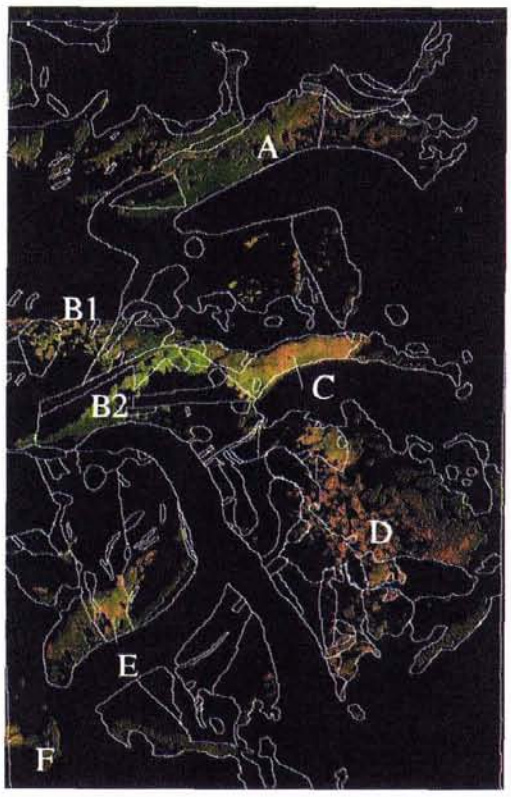

Plate 1. Landsat TM ratio composite. Red = 5/7, green = 3/1. A - F, locations discussed in text.

$$NV = (SV/MD) - 1 * 100$$

where NV is the normalized value, SV is the sample value, and MD is the median value of lithological unit.

Plates 2a and 2b are continuous surface maps showing the distribution of SiO_2 and alkali elements (alkali index), respectively. The location of geochemical samples are also shown. Both these maps have been normalized to lithology as discussed above.

Continuous surface maps for various trace elements, including Cu, Zn, Pb, Au, As, and Sb, were also produced to assist in establishing possible spatial relationships between alteration patterns present on the TM ratio images and precious metal and base metal mineralization. These continuous surface maps were combined into red-green-blue (RGB) color composite ternary images so the variations between trace elements could be clearly displayed as varying shades of the primary colors. Plate 3 is an RGB (red-green-blue) color ternary image in which continuous surface maps of Au, As, and Sb have been displayed in red, green, and blue colors, respectively. Consequently, areas high in Au, As, and Sb are displayed in bright red, green, and blue colors, respectively. Yellow areas represent fairly high concentrations of both Au and As (e.g., red + green) whereas white areas reflect high concentrations in all three trace elements (e.g., red + green + blue = white). Plate 4 is a similar map except that Cu, Zn, and Pb have been displayed through red, green, and blue colors, respectively.

Mapped Alteration Zones

Figure 2, taken from Kirkham and Margolis (1995), shows the location of major alteration zones as well as mineralized areas. The alteration zones include sericte (phyllic), chlorite, pyrite, argillite, quartz stockworks, and silicification (quartz veins) as well as zones of copper mineralization. This map was digitized so that the known alteration zones could be statistically and spatially compared to the TM ratio and lithogeochemical data. This was accomplished by employing the GIS to compare the ratio maps that were classified into standard deviation classes (as discussed above) with the mapped alteration zones shown on Figure 2. A map comparison procedure based on chi-squared statistics was used to measure the association between the data. An area cross-tabulation was calculated showing the observed and expected overlap between map classes, and a plot of the observed minus expected value for each ratio class versus alteration type were constructed (figures not shown).

Data Integration : Au and Cu Exploration Potential Maps

The capabilities of the GIS were employed to produce exploration potential maps for Au and Cu porphyry based on the TM and lithogeochemical data. GIS have been used by various geoscientists to produce mineral potential maps (Bonham-Carter *et al.*, 1988; Harris, 1989; Harris *et al.*, 1994; Rencz *et al.*, 1994b; Wright *et al.*, 1996). Bonham-Carter (1994) provides a particularly comprehensive overview of the use of GIS for the production of mineral potential maps.

Exploration in this area is focused on Cu-Mo porphyry deposits and epithermal Au deposits as mentioned in the section describing the characteristics of the study area. Therefore, indicators of these particular deposit types were selected for input to the modeling process. Table 1 lists the data used to produce the exploration potential maps as well as the relevance of each to the associated deposit model (e.g., Cu-Mo porphyry and epithermal Au). General descriptions of these mineral deposit types and relevant exploration criteria can be found in Evans (1993) and Guilbert and Park (1975) while specific discussions of mineralization styles in the study area can be found in Kirkham and Margolis (1995) and Margolis and Britten (1995).

Each data type listed in Table 1, in the form of a continuous surface map (image), was scaled from raw numbers (DN values for the TM ratios and either ppm or ppb for the lithogeochemical data) to numbers between 0 and 255 to standardize values for modeling purposes. With regards to exploration favorability, 255 and 0 represent the most and least favorable areas for exploration for each model, respectively. The values for the aklali index were reversed so that high values represent areas of alkali depletion because epithermal Au deposits are often associated with regions depleted in alkali elements as a result of hydrothermal alteration. The maps were then simply added together using an *index overlay* operation in the GIS, resulting in the final exploration favorability maps which are shown in Figures 7a and 7b for mesothermal-epithermal Au and Cu-Mo porphyry, respectively. Brighter tones represent areas more prospective for exploration.

Plate 5 is a ternary RGB map based on the lithogeochemical data which shows alteration patterns that may reflect underlying Cu and/or Au mineralization. The lithogeochemical data and associated alteration indicies comprising this composite image were chosen to identify potassic, phyllic-argillic (sericite), and propylitic (chlorite) zones typical of Cu porphyry deposits. Only areas of outcrop are displayed on this image.

Data Analysis

The following section discusses the patterns observed on the ratio maps (Figures 5a and 5b), color composite ratio image (Plate 1) produced from the TM data and their relationships to lithogeochemical data, and the mapped alteration zones shown on Figure 2.

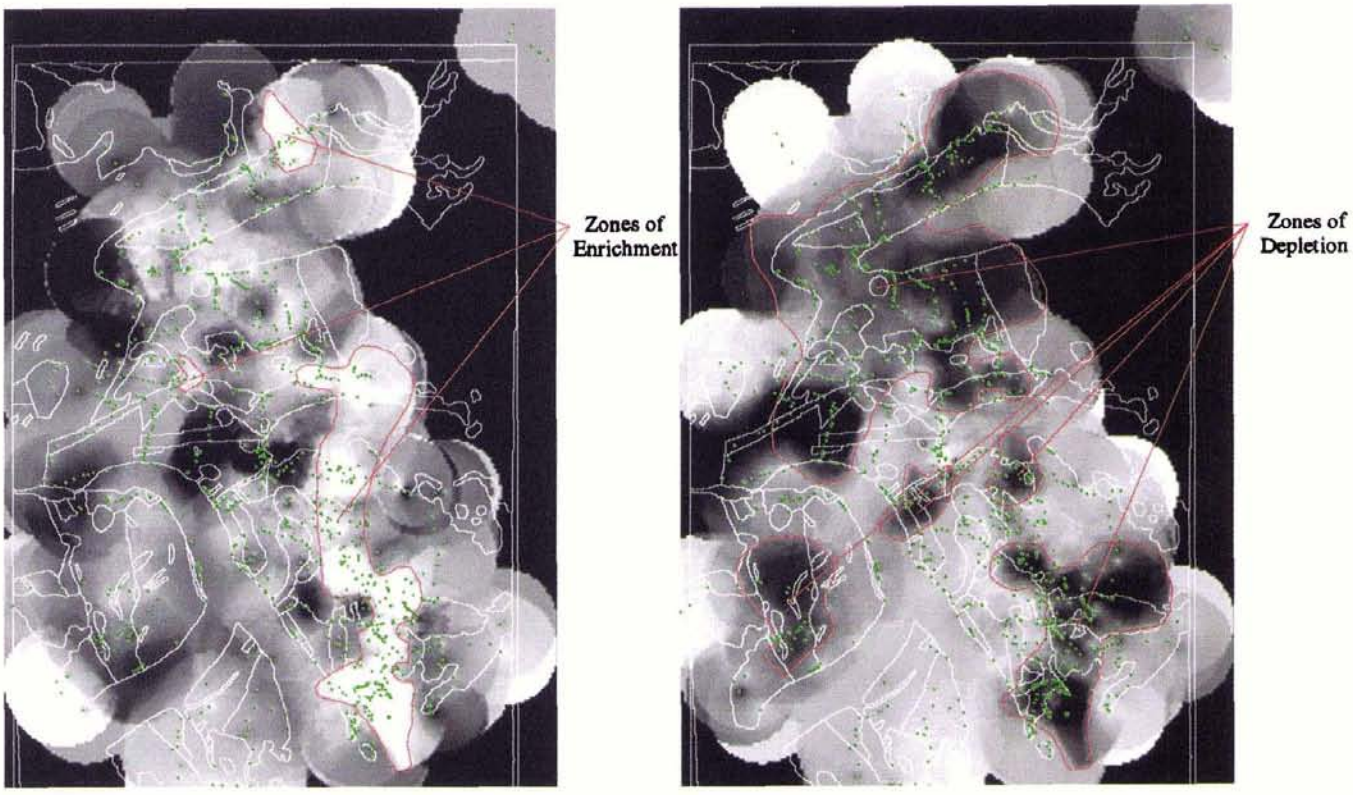

Plate 2. (a) SiO_2 - normalized. (b) Alkali index. Continuous surface maps of the geochemical data have been produced using an inverse distance weighted algorithm (IDW). In the case of (a), the lighter tones indicate higher SiO_2 values (%) while darker tones indicate lower values. The lighter tones in (b) reflect higher alkali index values (possible enrichment) while darker tones reflect lower values (depletion). Geochemical sample points (green dots) and lithological boundaries have been overlaid on these figures.

TABLE 1. DATA USED TO PRODUCE EXPLORATION FAVORABILITY MAPS SHOWN IN FIGURES 7a AND 7b

	Input Data	Information Provided
Mesothermal - Epithermal Au Primarily eastern portion of the study area	Landsat TM 5/7	phyllic (sericitic) to argillic alteration
	Au, As, Sb	possible mineralized areas
	Alkali Index $(Na_2O + CaO)/(Na_2O + K_2O + CaO)$	sodium depletion reflecting hydrothermal alteration
	SiO_2	silicification and quartz veining
	Sericite Index $(K_2O/Na_2O + K_2O)$	phyllic (sericitic) alteration
	Sulphur	delineate areas of high sulphur fugacity and acidic environments
Cu - Mo- (Au) Porphyry Primarily western portion of the study area	Landsat TM 3/1 ratio	iron staining (gossans)
	Cu, Mo	possible mineralized areas
	K_2O	potassic alteration
	Chlorite Index $(Fe_2O_3 + MgO)/Fe_2O_3 + MgO + CaO + Na_2O)$	propylitic alteration (chloritization)
	Iron Index (Fe_2O_3/FeO)	iron staining (oxidation) - gossans
	Sericite Index $(K_2O/Na_2O + K_2O)$	phyllic (sericitic) alteration

Ratio Maps

TM5/TM7

Figure 5a is a TM 5/TM 7 ratio image which shows areas of possible phyllic (sericitic) to argillic alteration. The strongest areas of alteration, indicated by the ratio image, occur just north of the Hanging Glacier on a south-facing slope within an area mapped as pyritic alteration as well as a broad zone south of the same glacier in the vicinity of Brucejack Lake (see Figures 1 and 2 for reference).

Figure 8 shows a series of exploratory box and whisker plots for SiO_2 concentration for the 5/7 ratio data. Figure 8a shows SiO_2 content for the TM 5/7 ratio map which has been divided into four reflectance classes as discussed above and summarized below:

- 1 ≤ mean 5/7 ratio value
- 2 = mean to 1 standard deviation (std. dev.)
- 3 = 1 to 2 std. dev.
- 4 ≥ 2 std. dev.

- 0 = non-outcrop or outcrop < 30m² (resolution of TM data)
- −9999 = outside study area

An increase can be seen in SiO_2 content over the areas characterized by higher TM 5/7 ratios. However, this observed trend is without regard to the individual lithologies which of course, depending on composition, could affect this apparent positive correlation between SiO_2 content and higher TM 5/7 ratio classes. Figures 8b and 8c show SiO_2 content for each TM 5/7 ratio class over the volcanic rocks (Unka River and Betty Creek Formations), and pyritic altered rocks (unit 3), respectively (see Figure 1 for geological units). The same positive trend is visible although it only appears statistically significant[1] for the highest TM 5/7 ratio class.

Similar exploratory analysis was applied to all elements (oxides) for both the TM 5/7 and 3/1 ratio maps for each lithology. Tables 2a and 2b summarize the lithogeochemical trends for the ratio classes for both the TM 5/7 and 3/1 ratio images, respectively. The highest TM 5/7 ratio class (class 4) comprised a population of 81 lithogeochemical sample points while the highest TM 3/1 ratio class contained 60 sample points.

The heavy black arrows in Table 2 indicate a significant relationship between the highest ratio class and the particular oxide element while the white arrows indicate a less significant correlation. The direction of the arrow indicates whether there is a positive or negative trend between the ratio class and the particular element. For example, when analyzing the ratio data without regard to individual rock units, there appears to be a significant increase in SiO_2 over areas with the highest TM 5/7 ratio, indicating that areas of more intense phyllic alteration are also characterized by more intense silicification. Decreasing trends in MgO, Al_2O_3, Na_2O, CaO, K_2O, and the chlorite, iron, and alkali indices and increasing trends in the sericite index, zinc, arsenic, and especially gold appear to be correlated with areas of more intense phyllic (serictic) alteration as indicated on the TM 5/7 ratio data. The same trends are evident when the effect of each lithology is taken into account although the alkali depletion trend is less significant in the pyritic altered rocks (unit #3).

Box and whisker plots (Figure 9a) of TM 5/7 ratio values for each of the known alteration types shown on Figure 2 indicate that zones mapped as sericite alteration, intense copper mineralization, and quartz enrichment (quartz veining) have the highest statistically significant 5/7 ratio values whereas the mapped areas of potassic alteration have the lowest 5/7 ratio values.

Chi-squared contingency tables showing the observed and expected overlap between the 5/7 ratio classes and the mapped alteration zones indicate that the largest degree of spatial overlap occurs between the sericte alteration zones and the higher 5/7 ratio values (especially classes 2 and 3 representing ratio values between the average ratio value and two standard deviations above the mean). Mapped sericite alteration zones and, to a lesser extent, pyritic alteration zones

[1]A significant statistical trend (e.g., distinct populations) is indicated when there is no overlap in the 95% confidence limits (demarcated by notches) in the box and whisker plots.

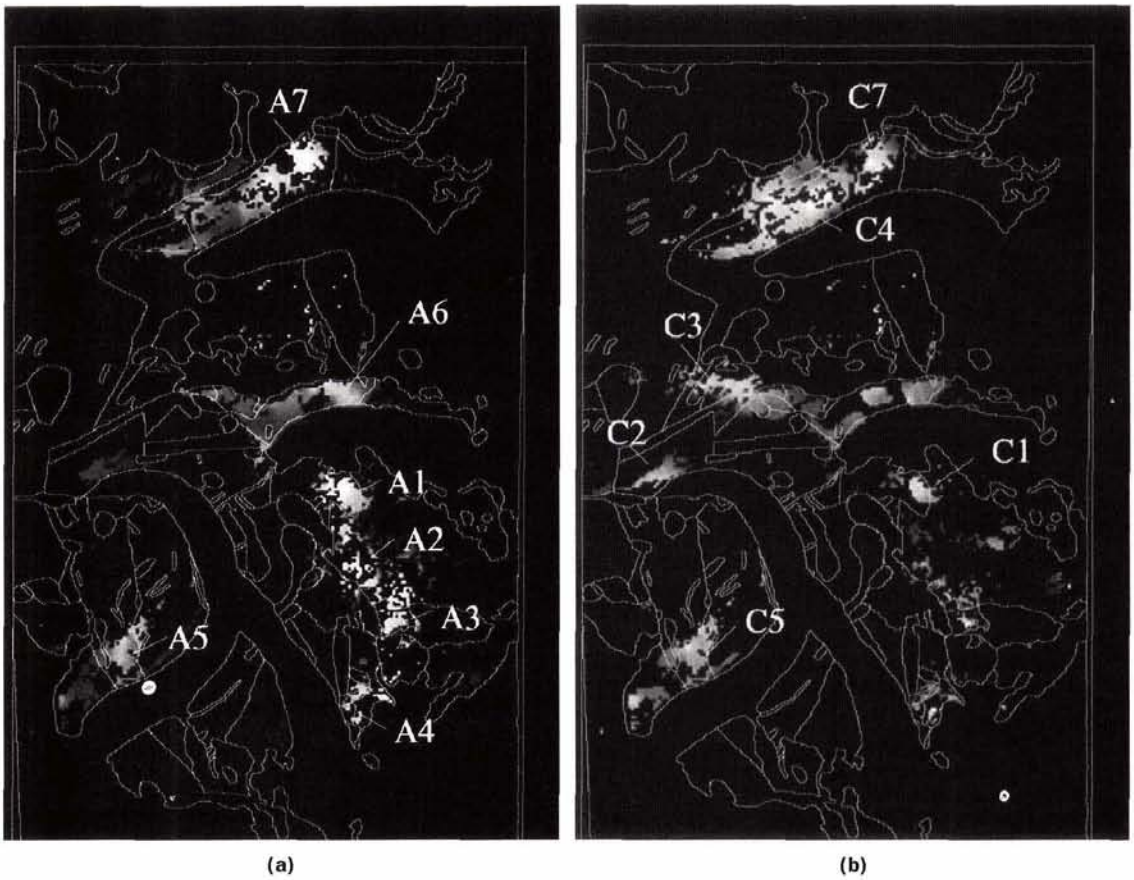

Figure 7. (a) Au potential map. A1 to A7, prospective zones (see text). (b) Cu porphyry potential map. C1 to C7, prospective zones (see text).

TABLE 2a. SUMMARY OF LITHOGEOCHEMICAL TRENDS FOR TM 5/7 DATA

Element	Trend - Entire Area	Geology #3	Geology #8	Highest Geological Unit (see Fig.1)	LEGEND
SiO2	↑ 3,4	↑	↑	#3 #8	#3 Pyritic Altered Rocks
Al2O3	↓ 3,4	↓	↓	#4	#8 Volcanics-Unka River & Betty Creek Formation
MgO	↓ 3,4	↓	↓	#10 #11	
K2O	↓ 3,4	∀	↓	#4	#4 Mitchell Intrusion-Syenite
Na2O	↓ 3,4	∀	↓	#4	#10 Volcanic Rocks
CaO	↓ 2,3,4	∀	↓	#10 #11	#11 Sedimentary Rocks
Fe2O3	----------				
FeO	----------				
TiO2	∀				↑↓ Significant positive /negative trends
Zn	↑ 4				∀ A Less significant trends
As	↑ 3,4				↑ 3,4 Refers to ratio class number (see text for discussion)
Ag	----------				
Au	↑ 4				------- No distinguishable trend
Pb	∀ 4				
Cu	↓ 2,3,4				
Sericite IND	↑				
Chlorite IND	∀				
Iron IND	----------				
Alkali IND	↓				

TABLE 2b. SUMMARY OF LITHOGEOCHEMICAL TRENDS FOR TM 3/1 DATA

Element	Trend - Entire Area	Geology #3	Geology #8	LEGEND
SiO2	A 4	A	x	#3 Pyritic Altered Rocks
Al2O3	A	----------	x	#8 Volcanics-Unka River & Betty Creek Formation
MgO	A	↑	x	
K2O	A	A	x	#4 Mitchell Intrusion-Syenite
Na2O	A	A	x	
CaO	↓ 2,3,4	↓	x	#10 Volcanic Rocks
Fe2O3	A	A	x	#11 Sedimentary Rocks
FeO	A	A	x	
TiO2	A	A	x	↑↓ Significant positive /negative trends
Zn	↑ 3,4			∀ A Less significant trends
As	----------			↑ 3,4 Refers to ratio class number (see text for discussion)
Ag	----------			
Au	----------			------- No distinguishable trend
Pb	∀			x Not enough samples to make a statistically reliable measurement
Cu	A 1,2			
Sericite IND	∀			
Chlorite IND	A			
Iron IND	A			
Alkali IND	↑			

show a higher than expected spatial overlap with the 5/7 ratio classes (classes 2, 3, and 4). The lowest degree of overlap with the 5/7 ratio classes occurs with zones of weak copper mineralization. Overlap between 5/7 ratio classes and zones of potassic alteration show no significant relationship.

TM3/TM1

Figure 5b is a TM 3/TM 1 ratio image which shows areas of possible iron oxidation. The brighter areas possibly represent areas of limonite staining reflecting iron sulphide oxidation. Comparison with Figure 2 indicates that much of the outcrop area occurs in the pyritic altered rocks. Areas of more intense limonite staining indicative of pyritic alteration exist to the northwest of the Hanging Glacier, a long west-southwest trending zone which in part co-occurs with the Sulphurets/ Montgomery mineralized zones, an area in the southwest overlapping the Kerr deposit and, to a lesser extent, north of the Mitchell Glacier over the Mitchell and Iron Cap mineralized zones and finally a small area south of the Hanging Glacier.

Stronger correlations appear to exist between the lithogeochemical data and the TM 5/7 ratio data as opposed to the TM 3/1 ratio image as indicated in Tables 2a and 2b. The only significant trends in the 3/1 data is a decrease in CaO and an increase in the alkali index and zinc (Table 2b). Less significant trends include an increase in Fe_2O_3 (reflecting iron oxidization from FeO to Fe_2O_3), SiO_2, chlorite, and iron indices and a decrease in the sericite index. The relationship between the lithogeochemical and TM 3/1 ratio data appear less significant, perhaps due to the general nature of the iron gossans which are non-homogeneous and characterized by disseminated iron pyrite intermixed with phyllic alteration.

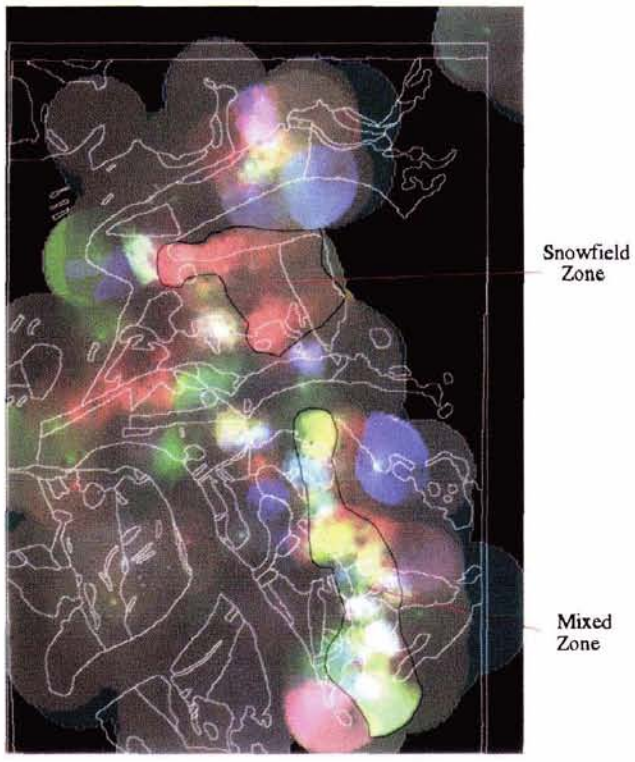

Plate 3. Precious metal composite. Red = Au, green = As, blue = Sb.

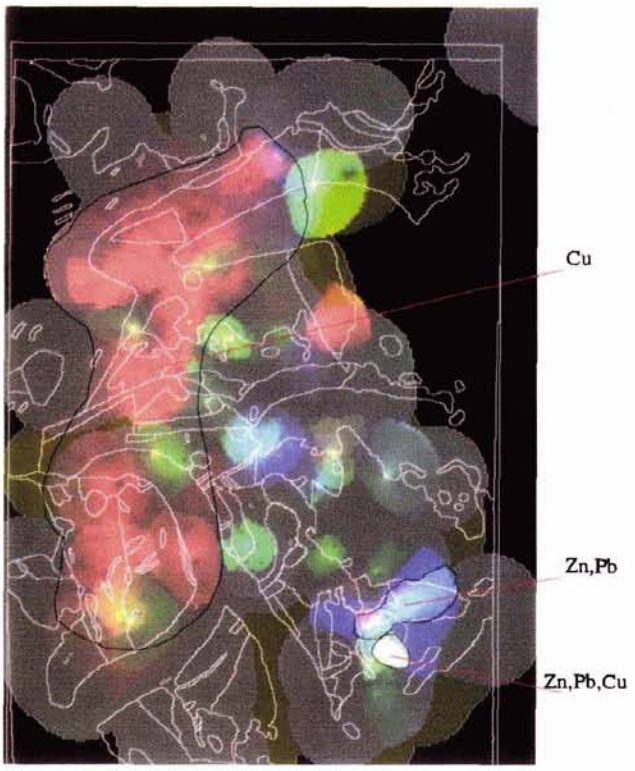

Plate 4. Base metal composite. Red = Cu, green = Zn, blue = Pb.

Thus, a unique spectral signature cannot be obtained from the TM data. The areas of phyllic alteration are much larger and more continuous throughout the study area, resulting in unique spectral signatures from the TM data. In general, the lithogeochemical trends associated with the TM 3/1 ratio image are generally weak with the exception of CaO depletion, and are opposite to those present for the TM 5/7 image.

Figure 9b shows box and whisker plots of TM 3/1 ratio values for each of the known alteration types shown on Figure 2. Zones mapped as intense copper mineralization and mineralized zones have the highest statistically significant 3/1 ratio values whereas the mapped areas of quartz enrichment have the lowest values.

A chi-squared contingency table showing the observed and expected overlap between the 3/1 ratio classes and the mapped alteration zones indictates that the largest degree of spatial overlap occurs between the two highest 3/1 ratio classes (> 1 std. dev. above the mean ratio value) and the intense copper and pyrite alteration zones. Both these mapped alteration zones have a higher than expected degree of overlap with the 3/1 ratio classes.

Combined TM Ratio Maps

A number of distinct linear zones characterized by different 5/7 and 3/1 ratio values can be seen on Plate 1. A zone north of the Mitchell Glacier ("A" on Plate 1) is characterized by a green color in the west portion, reflecting higher 3/1 ratios indicative of more intense iron oxidation. An east-west striking zone ("C") in the central portion of the study area is characterized by iron oxidation (pyrite alteration) in the

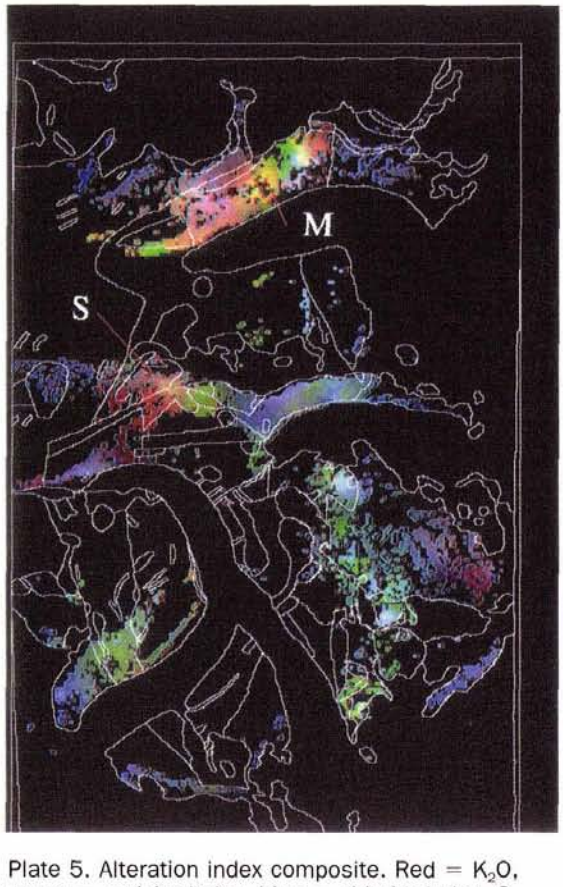

Plate 5. Alteration index composite. Red = K_2O, green = sericite index, blue = chlorite index. S and M are locations discussed in the text.

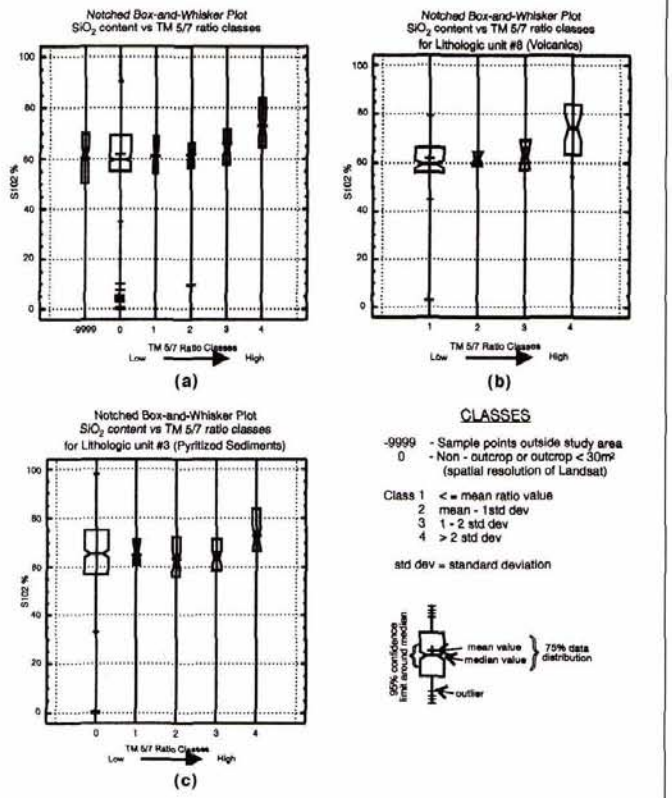

Figure 8. Box and whisker plots showing SiO_2 concentration for TM 5/7 ratio classes.

southwest portion of this zone and sericitic alteration and pyritic alteration (e.g., reddish-yellow) south of the Hanging Glacier on a steep south facing slope. The western portion of this linear zone bifurcates into a northern zone ("B1") dominated by reddish-yellow hues reflecting high 5/7 and 3/1 ratio values indicative of sericitic/pyritic alteration and a southerly zone ("B2") characterized by intense iron oxidation (pyritic alteration). This southern zone in part coincides with the Sulphurets mineralized zone. A broad zone located in the southeast portion of the study ("D") area in the vicinity of Brucejack Lake (Figure 1) is dominated by red hues indicative of strong phyllic (sericitic) alteration. The area in the vicinity of the Kerr Cu-Au deposit ("E") in the southwest portion of the study area as well as zone "F" are zones of mixed pyritic and sericitic alteration as reflected by the yellow-green hues.

Lithogeochemical Data

In order to evaluate the alteration trends spatially, continuous surface maps of the various oxide elements were constructed as previously discussed. A linear north-south striking zone of SiO_2 enrichment and alkali depletion is evident in the eastern portion of the study area over primarily volcanic rocks (Plates 2a and 2b). This represents a strong zone of intense silicification (quartz veining) and phyllic (sericitic) alteration. Spatially, this reflects the statistical trends evident in the TM 5/7 ratio because large areas of outcrop occur over this zone (see Figure 5a). This zone may be related to faulting because it is quite linear and strikes north-south paralleling many mapped faults (e.g., Brucejack Lake Fault - Figure 2).

A strong linear zone of Au and As enrichment (yellow) and Au, As, and Sb enrichment (white) seen on Plate 3 corresponds directly with the linear zone of intense silicification, sericitic alteration, and alkali depletion observed in Plates 2a and 2b. Plate 4 is dominated by elevated levels of copper (bright red areas) in the western portion of the study over primarily pyritic altered rocks (see Figure 2). These two images indicate that two mineralizing systems may be present in the area: the western half is dominated by a base metal system characterized by elevated levels of Cu with a less dominant precious metal system reflected by sporadic areas with elevated Au, while the eastern half of the study area is characterized by a precious metal (primarily gold) system. These qualitative observations based on visual interpretation of the above images are quantitatively verified in Table 3 which shows that the eastern half of the study area is characterized by significantly higher SiO_2, Au, As, Ag, Sb, and sulphur values but lower Cu, FeO, Fe_2O_3, and CaO values.

The alteration patterns derived from analysis of the TM data shown in Figure 5 and Plate 1 appear to generally reflect this apparent division. The red hues on Plate 1, representing more intense silicification, phyllic (sericitic), and in some localized areas argillic alteration, tend to dominate the eastern portion of the study area over primarily volcanic rocks. These areas are characterized by elevated levels of Au, As, and Sb as shown in Plate 3. One area of fairly intense sericitic and pyritic alteration, characterized by strong iron oxidation (e.g., red + green = yellow), occurs within this zone southeast of the Golden Marmot district (see Figure 2).

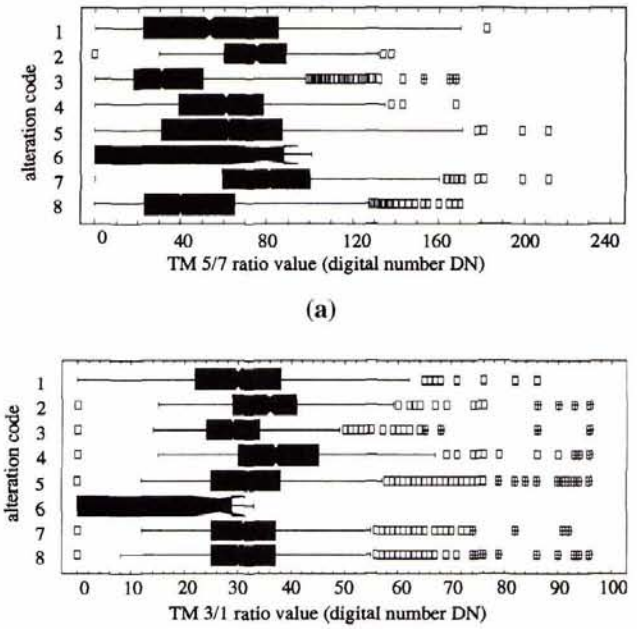

Figure 9. Box and whisker plots showing TM ratio values for each alteration zone shown on Figure 2. (a) TM 5/7 ratio versus mapped alteration zones. (b) TM 3/1 ratio versus mapped alteration zones.

TABLE 3. MAJOR OXIDE AND SELECTED TRACE ELEMENT MEAN VALUES FOR THE EAST AND WEST HALF OF THE STUDY AREA (VALUES FOR MAJOR ELEMENTS IN WEIGHT %, TRACE ELEMENTS IN PPM EXCEPT FOR AU WHICH IS IN PPB)

	SiO_2	Al_2O_3	K_2O	CaO	FeO	Fe_2O_3	Zn	Sb	Au	As	Ag	Cu	S
East	70.6	12.7	4.1	1.3	1.7	2.2	245	49.1	219.3	139.5	59.4	64.4	5029.6
West	59.5	15.3	4.8	2.1	2.7	3.3	282	24.6	180.5	64.7	12.2	893.7	3962

TABLE 4. SUMMARY OF SALIENT CHARACTERISTICS OF HIGH POTENTIAL ZONES FOR AU AND CU PORPHYRY EXPLORATION AS DETERMINED BY GIS MODELING METHODS (SEE TABLE 1 AND FIGURES 7a AND 7b AND PLATE 5) (A = AU AND C = CU PORPHYRY)

Identification # (see Fig. 7a,b)	Mineralized Zone (see Fig. 2)	Lithogeochemical Characteristics (from Plate 5)	Landsat TM Ratio Characteristics (from Fig. 5 & Pl. 1)
A1/C1	Golden Marmot	sericite and chlorite alteration	mixed phyllic (sericitic) alteration (5/7) and iron staining (3/1)
A2	Golden Rocket	sericite alteration	phyllic alteration (5/7)
A3	Brucejack Lake	sericite and chlorite alteration	phyllic alteration (5/7)
A4	West Zone	sericite and weak potassic alteration	phyllic alteration (5/7)
A5/C5	Kerr	sericite and weak potassic alteration	mixed phyllic (sericitic) alteration (5/7) and iron staining (3/1)
A6	Josephine	sericite and chlorite (weak) alteration	mixed phyllic (sericitic) alteration (5/7) and iron staining (3/1)
A7/C7	Iron Cap	potassic and sericite alteration	mixed phyllic (sericitic) alteration (5/7) and iron staining (3/1)
C2	Sulphurets Lake	sericite (weak) and chlorite alteration	strong iron staining (3/1)
C3	Sulphurets	potassic to phyllic to propylitic (chlorite) alteration forming a zoned pattern	strong iron staining (3/1)
C4	Mitchell	potassic and sericite alteration	strong iron staining (3/1)

Conversely, Plate 1 shows that areas of more intense pyritic alteration (iron oxidation), displayed in green, tend to occur in the western half of the area over the pyritic altered rocks correlating with elevated levels of copper seen on Plate 4.

Discussion: Implications for Mineral Exploration

The higher 5/7 ratio values appear to reflect more intense zones of phyllic (quartz-sericite-pyrite) alteration where sericite and quartz are the dominant components. These areas are characterized by significant increases in SiO_2 (quartz veining due to late-stage hydrothermal alteration) and strong alkali (Na_2O, K_2O) and CaO and MgO depletion. The higher 3/1 ratio values also appear to reflect zones of phyllic alteration but with a stronger pyritic (iron gossan) alteration component and significant CaO depletion.

Spatially, the TM ratio data (see Figure 5 and Plate 1) appear to reflect two alteration styles, one dominated by more intense iron oxidation (pyritic) occurring more predominately in the eastern portion of the study area (Sulphurets, Montgomery, Mitchell, and Iron Cap mineralized zones) and the other dominated by more intense sericitic and silicification occurring in the southeast portion of the study area in the vicinity of Brucejack Lake south of the Hanging Glacier. These different alteration styles may reflect different mineralization systems, the east dominated by a copper-gold porphyry system while the east by a mesothermal-epithermal precious metal (particularly Au) system high in sulphur (see Table 3). This tentative conclusion is supported by the higher copper values in the western portion of the study area and generally higher gold values in the eastern portion (see Plates 3 and 4) and by models proposed by Margolis and Britten (1995).

Figures 7a and 7b are epithermal Au and Cu porphyry exploration potential maps produced using the GIS as discussed previously. With respect to Au potential, the zones of highest potential are restricted to the eastern portion of the study area and form a north-south striking zone paralleling, and in close proximity to, the Brucejack Lake Fault (see Figure 2). The apparent spatial association between these zones and the Brucejack Lake Fault may suggest a causal relationship with the fault providing a channel for hydrothermal fluids. With respect to Cu potential, most of the high potential zones occur west of the Brucejack Fault, although one zone (Golden Marmot) occurs east of this fault. Table 4 presents a summary of the the high potential zones, most of which are known and are associated with areas that have been explored or are presently being explored. Lesser known zones, determined from the TM ratio data and characterized by strong sericitic-pyritic alteration, include zone F in the extreme southwestern portion of the study area and zone B1 (see Plate 1) west of the Sulphurets zone in close proximity to a monzonite intrusion (Mitchell intrusion).

Plate 5, an RGB ternary image based on the lithogeochemical data as discussed previously, shows a number of notable alteration patterns. The Mitchell area ("M" on Plate 5) shows areas of mixed potassic (red), sericite (green), and mixed potassic/sericite (yellow) alteration. A distinct alteration pattern comprising a potassic core (red) and outer sericite/potassic (yellow) and propylitic (chlorite-green) zones, typical of Cu-Mo porphyry deposits, occurs in the Sulphurets zone ("S").

Summary and Conclusions

The success of the ratioing techniques presented in this paper depends not only on the amount of exposed bedrock, keeping in mind the 30-m resolution of TM data, but also on the "quality" of the outcrop and the degree of rock alteration.

It is clear from this study that the Cordilleran region of British Columbia is suitable for the application of these processing techniques. Sufficient exposed un-altered and altered outcrop is available so that reliable spectral signatures can be obtained from the TM data, allowing the use of image processing techniques (in this case simple ratio images) to detect and map altered rocks. Application of these techniques would be less successful in areas typifying the Precambrian Shield due to glacial and vegetative cover and less extensive areas of fresh outcrop. These techniques could be applied in

arctic environments because extensive areas of outcrop are present; however, lichen cover would tend to reduce the likelihood of obtaining reliable spectral signatures from the TM data.

In general, pyritic alteration characterized by areas of iron oxidation (pyrite-sericite) and areas of intense phyllic (sericite-pyrite) alteration could be distinguished on the TM ratio images. Combination of the two alteration types could also be determined on a color composite of the ratio images (Plate 1). The fairly dense survey of lithogeochemical data enabled the alteration zones identified on the TM data to be calibrated with respect to major oxide element trends. Furthermore, the lithogeochemical data added further detail on the chemical nature of many of the alteration zones characterized by potassic, phyllic, and propylitic alteration. These alteration styles reflect the underlying rock type, as would be expected, but also appear to reflect two different styles of alteration, reflecting different mineralizing systems as indicated on the RGB trace element maps (Plates 3 and 4). The western half of the area, characterized by more intense iron-pyritic alteration, reflects a base metal (Cu porphyry and minor Au) system while the eastern half, characterized by areas of silicification and sericitic-pyritic alteration, may represent a precious metal (Au, As, Sb) system.

Although this study has been conducted over a relatively small area, these techniques could be applied over much wider areas covered by several TM images. Analysis of TM data in the Cordilleran environment of British Columbia represents an effective technique for the regional targeting of anomalies worthy of exploration follow-up. Considering that much of the area is only accessible by air and that TM data are relatively inexpensive, the techniques presented in this paper could form an important part of regional exploration programs in the Cordillera.

References

Abrams, M.J., R. Ashley, L. Rowan, A. Goetz, and A. Kahle, 1977. Mapping of hydrothermal alteration in the Cuprite Mining District, Nevada, using aircraft scanner images for the spectral region 0.46 to 2.36 μm, *Geology*, 5:713–718.

Abrams, M.J., J.W. Conel, and H.R. Lang, 1984. *The Joint NASA/Geosat Test Case Project, Final Report, Part 2, Vol. 1* (H.N. Paley, editor), American Association of Petroleum Geologists, Oklahoma.

Alldrick, D.J., and J.M. Britton, 1988. *Geology and Mineral Deposits of the Sulphurets Area*, Open File Map 1988-4 (1:50,000), Ministry of Energy, Mines and Petroleum Resources, Province of British Columbia.

Ballantyne, S.B., 1990. Geochemistry of Sulphurets area, British Columbia, *Program with Abstracts, GSC Minerals Colloquium*, Ottawa, 17-18 January, p. 14.

Ballantyne, S.B., and J. Ma, 1992. LANDSAT Thematic Mapper with ground truth element distribution: An example from British Columbia Golden Triangle District, *Program with Abstracts, GSC Forum 92*, Ottawa, p. 3.

Bridge, D.J., 1993. *The Deformed Early Jurassic Kerr Copper-Gold Porphry Deposit, Sulphurets Gold Camp, Northwestern British Columbia*, unpublished M.Sc. thesis, The University of British Columbia, Vancouver, British Columbia, 303 p.

Bonham-Carter, G.F., 1994. *Geographic Information Systems for Geoscientists: Modeling with GIS*, Pergamon (Elsevier Science Ltd.), 398 p.

Bonham-Carter, G.F., F.P. Agterberg, and D.F. Wright, 1988. Integration of geological datasets for gold exploration in Nova Scotia, *Photogrammetric Engineering & Remote Sensing*, 54(11):1585–1592.

Buckingham, W.F., and S.E. Sommer, 1983. Mineralogical characteristics of a rock surface formed by hydrothermal alteration and weathering — an application of remote sensing, *Economic Geology*, 78:664–674.

Campbell, J.B., 1987. *Introduction to Remote Sensing*, Guilford Press, New York, 551 p.

Crippen, R.E., 1987. The regression intersection method of adjusting image data for band ratioing, *International Journal of Remote Sensing*, 8:137–155.

———, 1988. The dangers of underestimating the importance of data adjustments in band ratioing, *International Journal of Remote Sensing*, 9(4):767–776.

Davis, J.C., 1986. *Statistics and Data Analysis in Geology*, John Wiley and Sons, New York, 645 p.

Drury, S.A., 1987. *Image Interpretation in Geology*, Allen and Unwin, London, 243 p.

Elvidge, C.D., and R.J.P. Lyon, 1984. Mapping clay alteration in the Virginia Range-Comstock Lode, Nevada with airborne thematic mapper imagery, *Proceedings, International Symposium on Remote Sensing of the Environment, 3rd Thematic Conference for Exploration Geology*, pp. 61–170.

Evans, A.M., 1993. *Ore Geology and Industrial Minerals: An Introduction*, Blackwell Science, Cambridge, Massachusetts, 389 p.

Evenchick, C.A., 1991. Geometry, evolution, and tectonic framework of the Skeena Fold Belt, north central British Columbia, *Tectonics*, 10:527–546.

Fowler, B.P., and R.C. Wells, 1996. The Sulphurets Gold Zone, Northwestern British Coloumbia, *Porphry Deposits of the Northwestern Cordillera of North America* (T.G. Schroeter, editor), Canadian Institute of Mining, Metallurgy and Petroleum, Special Volume 46, Paper 35.

Gibson, H., W. MacLean, B. Taylor, and G. Prior, 1994. *Lithogeochemical and Isotopic Techniques in the Exploration for Volcanic Massive Sulphide Deposits*, CIM Geological Society Field Conference - Short Course 2.

Goetz, A.F.H., 1989. Spectral Remote Sensing in Geology, *Theory and Applications of Optical Remote Sensing* (G. Asrar, editor), John Wiley and Sons, pp. 491–526.

Guilbert, J.M., and C.F. Park, 1986. *The Geology of Ore Deposits*, W.H. Freeman and Co., New York, 985 p.

Harris, D.C., and S.B. Ballantyne, 1992. Ore mineralogy and lithogeochemistry of the Mitchell-Sulphurets District, potassic high-sulphur precious metal system, *Program with Abstracts, GSC Minerals Colloquium*, Ottawa, 22-24 January, p. 19.

Harris, J.R., 1989. Data integration for gold exploration in eastern Nova Scotia using a GIS, *Proceedings of Remote Sensing for Exploration Geology*, Calgary, Alberta, pp. 233–249.

Harris, J.R., L. Wilkinson, and J. Broome, 1995. Mineral exploration using GIS-based favourability analysis, Swayze Greenstone Belt, Northern Ontario, *Proceedings of the Canadian Geomatics Conference* (CD-ROM), National Defense.

Henderson, J.R., R.V. Kirkham, M.N. Henderson, J.G. Payne, W.O. Wright, and R.L. Wright, 1992. Stratigraphy and structure of the Sulphurets area, British Columbia, *Current Research, Part A*, Geological Survey of Canada, Paper 92-1A, pp. 323–332.

Hunt, G.R., and R.P. Ashley, 1979. Spectra of altered rocks in the visible and near infrared, *Economic Geology*, 74:1613–1629.

Johnson, R.A., and D.W. Wichern, 1982. *Applied Multivariate Statistical Analysis*, Prentice-Hall, New Jersey.

Kirkham, R.V., 1963. *The Geology and Mineral Deposits in the Vicinity of the Mitchell and Sulphurets Glaciers, Northwestern British Columbia*, unpublished M.Sc. thesis, University of British Columbia, Vancouver, B.C., 122 p.

Kirkham, R.V., S.B. Ballantyne, and D.C. Harris, 1990. Geology, geochemistry and mineralogy of a deformed porphyry copper molybdenum and precious metal system, *Program with Abstracts, GSC Minerals Colloquium*, Ottawa, 22-24 January, p. 11.

Kirkham, R.V., S.B. Ballantyne, D.C. Harris, J.R. Henderson, M.N. Henderson, and T.O. Wright, 1992. Lower Jurassic Sulphurets porphyry Cu-Au system Northwest British Columbia, *Program with Abstracts, GSC Minerals Colloquium*, Ottawa, 22-24 January, p. 3.

Kirkham, R.V., and J. Margolis, 1995. Overview of the Sulphurets area, northwestern British Columbia, *Porphry Deposits of the Northwestern Cordillera of North America* (T.G. Schroeter, edi-

tor), Canadian Institute of Mining, Metallurgy and Petroleum, Special Volume 46, Paper 34.

Krohn, M.D., 1986. Spectral properties (0.4 to 35 microns) of selected rocks associated with disseminated gold and silver deposits in Nevada and Idaho, *Journal of Geophysical Research*, 91(B1):767–783.

Ma, J., V.R. Slaney, J. Harris, D. Graham, S.B. Ballantyne, and D.C. Harris, 1988. Use of LANDSAT TM data for the mapping of limonitic and altered rocks in the Sulphurets area, central British Columbia, *Proceedings of the 14th Canadian Symposium on Remote Sensing*, Calgary, Alberta, pp. 419–422.

Margolis, J., 1993. *Geology and Intrusion-Related Copper-Gold Mineralization, Sulphurets, British Columbia*, unpublished Ph.D. dissertation, The University of Oregon, Eugene, Oregon, 289 p.

Margolis, J., and R.M. Britten, 1996. Porphyry-style and epithermal copper molybdenum-gold-silver mineralization in the northern and southeastern Sulphurets district, northwestern British Columbia, *Porphry Deposits of the Northwestern Cordillera of North America* (T.G. Schroeter, editor), Canadian Institute of Mining, Metallurgy and Petroleum, Special Volume 46, Paper 36.

Marsh, S.E., and J.B. McKeon, 1983. Integrated Analysis of High-Resolution Field and Airborne Spectroradiometer Data for Alteration Mapping, *Economic Geology*, 78:618–632.

Miller, N.L., and D.E. Elvidge, 1985. The iron absorption index: A comparison of ratio-based and baseline-based techniques for the mapping of iron oxides, *Proceedings of the Fourth Thematic Conference on Remote Sensing for Exploration Geology*, San Francisco, California.

Rencz, A., J. Harris, and S.B. Ballantyne, 1994a. LANDSAT TM imagery for alteration identification, *Current Research 1994-E*, Geological Survey of Canada, pp. 277–282.

Rencz, A.N., J.R. Harris, G.P. Watson, and B. Murphy, 1994b. Data integration for mineral exploration in the Antigonish Highlands, Nova Scotia: Application of GIS and remote sensing, *Canadian Journal of Remote Sensing*, 20(3):257–267.

Rowan, C., and E.H. Lathram, 1980. Mineral Exploration, *Remote Sensing in Geology* (Chapter 17) (B.S. Siegal and A.R. Gillespie, editors), John Wiley and Sons, New York. 702 p.

Sabins, F., 1996. *Remote Sensing Principles and Interpretation, Third Edition*, W.F. Freeman and Co., New York.

Wright, D.F., and G.F. Bonham-Carter, 1996. VHMS favourability mapping with GIS-based integration models, Chisel Lake - Anderson Lake area, *EXTECH 1: A Multidisciplinary Approach to Massive Sulphide Research in Rusty Lake - Snow Lake Greenstone Belts, Manitoba* (G.F. Bonham-Carter, A.G. Gally, and G.E.M. Hall, editors), GSC Bulletin 426, pp. 339–376, 387–401.

(Received August 1996; revised and accepted 18 June 1997; revised 21 August 1997)